Polym. Bull. (2018) 75:1895–1914
https://doi.org/10.1007/s00289-017-2128-6

ORIGINAL PAPER

Novel poly(vinyl chloride) nanocomposite films containing α-Al_2O_3 nanoparticles capped with vitamin B_1: preparation, morphological, and thermal characterization

Shadpour Mallakpour[1,2] · **Zahra Reisi**[1]

Received: 27 January 2017 / Revised: 18 June 2017 / Accepted: 13 July 2017 /
Published online: 18 July 2017

Abstract Many studies have been accomplished in the field of nanocomposite (NC) preparation to control the adhesion and spatial dispersion of nano-fillers and effect of these on attributes of the polymer matrix. In this investigation, surface modification of α-Al_2O_3 nanoparticles (NPs) was performed by vitamin B_1 (VB_1) as biodegradable and environmentally friendly modifier agent. Poly(vinyl chloride) (PVC) NCs were prepared with several contents of modified α-Al_2O_3 NPs (3, 5, and 7 wt.%) by ultrasonication method. Then, many standard techniques were used to study the properties of NC films. The results demonstrated that PVC/α-Al_2O_3–VB_1 NC films had better thermal stability and stress strength properties than pure PVC. Morphology images of PVC/α-Al_2O_3–VB_1 NCs showed the good dispersion of NPs in the polymer matrix in nanometer scale. They revealed that the α-Al_2O_3 NPs have sphere-like morphology. The mechanical properties of PVC/α-Al_2O_3–VB_1 NCs were improved by adding different amounts of α-Al_2O_3–VB_1 into the matrix of PVC. Water contact angle analysis showed increase in hydrophilicity of PVC/α-Al_2O_3–VB_1 NCs.

Keywords α-Al_2O_3 nanoparticles · Biocompatibility · Surface modification · Nanocomposites · Contact angle · Tensile properties

✉ Shadpour Mallakpour
mallak@cc.iut.ac.ir; mallak777@yahoo.com; mallakpour84@alumni.ufl.edu

[1] Organic Polymer Chemistry Research Laboratory, Department of Chemistry, Isfahan University of Technology, Isfahan 84156-83111, Islamic Republic of Iran

[2] Nanotechnology and Advanced Materials Institute, Isfahan University of Technology, Isfahan 84156-83111, Islamic Republic of Iran

Introduction

Nanocomposites (NCs) are materials designed for enhanced performance in any number of unique applications: structural, functional or cosmetic. NCs include a matrix, composed of polymer, metal or ceramic combined with nanoparticles (NP)s in suspension [1].

NPs have unparalleled chemical, mechanical, thermal, and electrical properties that make them very noteworthy for application in medicine, biotechnology, and environment-related initiatives.

Metal oxide NPs deputize a new class of substantial materials that are being developed for use in research, as a facility for functional materials of electrical and mechanical parts [2, 3].

Alumina NPs have attracted much interest because alumina is one of the cost-effective NPs that has hardness and high strength. α-Al_2O_3 NPs have supreme dielectric properties, good thermal conductivity [4], wear resistance [5], resistance to intense alkali, and acid attack at high temperatures. They have been used as nano-fillers for polymer NCs to improve the mechanical and conductive attributes [6, 7]. Among different forms of this worthwhile material, the ultrafine α-Al_2O_3 powder has considerable potential for a wide range of requisitions as high-strength materials, catalysts, and electronic ceramics [8, 9]. The wide utilization of ultrafine α-Al_2O_3 makes it a general material and increases the attention [10, 11].

NPs have an extremely high tendency of aggregation [11], due to the fact that they have small particle size and high surface energy [3, 12]. Dispersion of NPs in organic polymers can elevate a wide domain of material properties, such as mechanical and thermal properties as well as fire retardancy and barrier properties [5, 13]. One method to overcome aggregation of NPs is the use of different biocompatible coupling agents such as citric acid and ascorbic acid (vitamin C) [5, 14]. This is an efficacious method due to the strong covalent and hydrogen bonds created between the polymer chains and surface-modified NPs [15–18]. Another method is the use of ultrasound wave energy [19, 20]. Researches showed that the use of ultrasonic waves can improve the distribution of the NPs, control size distribution, morphology and decrease the aggregation in the polymer matrix [21, 22].

In this study, surface modification of α-Al_2O_3 NPs was accomplished by vitamin B_1 (VB_1) as a biocompatible modifier to enhance the dispersibility and prevent agglomeration. VB_1 (also called thiamine), has appeared as an eco-friendly, inexpensive, naturally occurring, and water-soluble compound with the reported toxicity parameter [LD_{50} (VB_1, oral rat) = 3710 mg/kg]. VB_1 is a pyrimidine derivative with a methylene-bridged thiazole moiety [23, 24]. The use of VB_1 analogs has been reported as powerful catalysts for different organic transformations [25].

Poly(vinyl chloride) (PVC) is one of the polymers with the highest production and applications due to its characteristics such as easy modification and low cost [26].

PVC has been reinforced with various fillers including titanium dioxide (TiO_2) [27], zinc oxide (ZnO) [28], iron oxide (Fe_3O_4) [29], and silver (Ag) [30] NPs for different purposes [31]. In this project, PVC/α-Al_2O_3–VB_1 NCs containing α-Al_2O_3–VB_1 NPs (3, 5, and 7 wt.%) were prepared by ultrasonic irradiation. The PVC/α-Al_2O_3–VB_1 NCs were characterized by techniques such as Fourier transform infrared (FT-IR) spectroscopy, X-ray diffraction (XRD), thermogravimetric analysis (TGA), and ultraviolet–visible (UV–Vis) spectroscopy. Field emission scanning electron microscopy (FE-SEM) and transmission electron microscopy (TEM) analyses were used to determine the morphology of the α-Al_2O_3–VB_1 and PVC/α-Al_2O_3–VB_1 NCs.

Experimental

Materials

α-Al_2O_3 powder (average particle size: 80 nm and purity: 99%) was supplied from Neutrino Co. (Tehran, I. R. Iran). VB_1 ($C_{12}H_{17}N_4OS$, Mw: 265.35 g/mol) was purchased from Alfa Aesar Co. (Karlsruhe, Germany). Emulsion (E)-PVC grade ($(C_2H_3Cl)_n$, Mw: 78.000 g/mol) was obtained from LG Chem Co. (Seoul, Korea). Tetrahydrofuran (C_4H_8O, Mw: 72.11 g/mol) was supplied by JEONG wang Co. (Gyeonggi-do, Korea).

Characterizations

The functionalization of α-Al_2O_3 NPs and fabrication of NCs were accomplished using Topsonics ultrasonic liquid processors (Tehran, I. R. Iran) with a frequency of 25 kHz and power of 100 W. The FT-IR spectra of the samples were recorded in a Jasco-680 (Japan) spectrophotometer in the form of KBr pellets of finely ground samples. It was used to study the characteristic peaks related to the NC films directly. The UV–Vis spectra were investigated by Jasco V-750 UV–Vis–NIR spectrophotometer (Tokyo, Japan), in the wavelength scan range from 200 to 800 nm.

XRD patterns were recorded on a Philips X'Pert MPDX-ray (Germany) diffractometer by a copper target operating at a voltage of 40 kV, a current of 35 mA, and Cu Kα radiation ($\lambda = 1.5418$ Å) over Bragg's angles (2θ) ranging from 10° to 80° with a scanning rate of 0.05 °C/min. Field emission scanning electron microscopy (FE-SEM) was performed on Hitachi S-4160 (Japan) instrument at an acceleration voltage of 15 kV. Prior to analysis, the composites were coated with an ultrathin gold layer in sputter coating method. TEM was done with a Philips CM120 microscope (Germany) (accelerating voltage 150 kV). Tensile testing was performed at room temperature on Hounsfield test equipment H25KS (RHI 5DZ, England). Tests were done with the speed of 5 mm/min. Contact angle measurements were done with U-vision MV500 digital camera microscope (China).

Surface modification of α-Al_2O_3 NPs with VB_1

The surface of α-Al_2O_3 NPs was treated with VB_1, 0.1 g of α-Al_2O_3 nanopowder was suspended into deionized (DI) water (8 ml) and ultrasonicated for 30 min. Then, 0.01 g of green modifier VB_1 (10% mass fraction of α-Al_2O_3 content) was dissolved in DI water (5 ml) by ultrasonication for 15 min. In the next step, the mixture of NPs and VB_1 solutions was sonicated for 30 min. Finally, the prepared suspension was dried at room temperature to obtain the powder of modified α-Al_2O_3 NPs with VB_1 (α-Al_2O_3–VB_1 NPs). The reaction sequences are shown in Scheme 1.

Preparation of PVC/α-Al_2O_3–VB_1 NC films

The preparation of PVC/α-Al_2O_3–VB_1 NC films was achieved by the following procedure: 0.10 g of PVC was added to 5 mL of THF by stirring (1 h at 40 °C). After that, different amounts of α-Al_2O_3–VB_1 (3, 5, and 7 wt.% of PVC) were separately added to PVC solution. Prepared mixtures were ultrasonicated for 30 min. Finally, the resulting suspensions were poured into glass Petri dishes and allowed to dry (Scheme 2). After evaporation of THF, NC films with high transparency were obtained that were easily separated from the Petri dishes (Fig. 1). The images of the prepared NC films with different contents of NPs are shown in Fig. 1. As it can be seen, transmission capability of PVC decreased with increasing the α-Al_2O_3–VB_1 NP contents.

Results and discussion

Modification of α-Al_2O_3 and composites preparation

VB_1 is utilized as a biocompatible modifier for creating more functional groups on the NPs' surface to prevent agglomeration, enhance the dispersibility and good miscibility of NPs in the PVC NCs. Based on performed study and recent investigations, the optimum weight percent of modifier was estimated around 10 wt.% [32]. In the modifying process, the amount of modifier is important because low amount of modifier can cause an inhomogeneous and low miscibility between the α-Al_2O_3 and the PVC matrix while, high amount of modifier can increase agglomeration of the NPs in PVC/α-Al_2O_3–VB_1 NC. Lone-pair electrons of chlorine atoms made many interactions in PVC. PVC has been used as a polymer matrix for the formation of the NCs [33]. The aim of this research is the manufacture of the NCs without aggregation of NPs in the polymer matrix. To overcome this problem, the environmentally friendly modifier and ultrasonic vibration were used. Ultrasonic power apparatus produces acoustic capitations and thereby affects the reaction. It makes bubble and these bubbles help to distribute the energy. In the modified α-Al_2O_3, the organic structure of VB_1 expands NPs' properties as filler. It gives a good ability to form homogeneous hybrid film with PVC matrix.

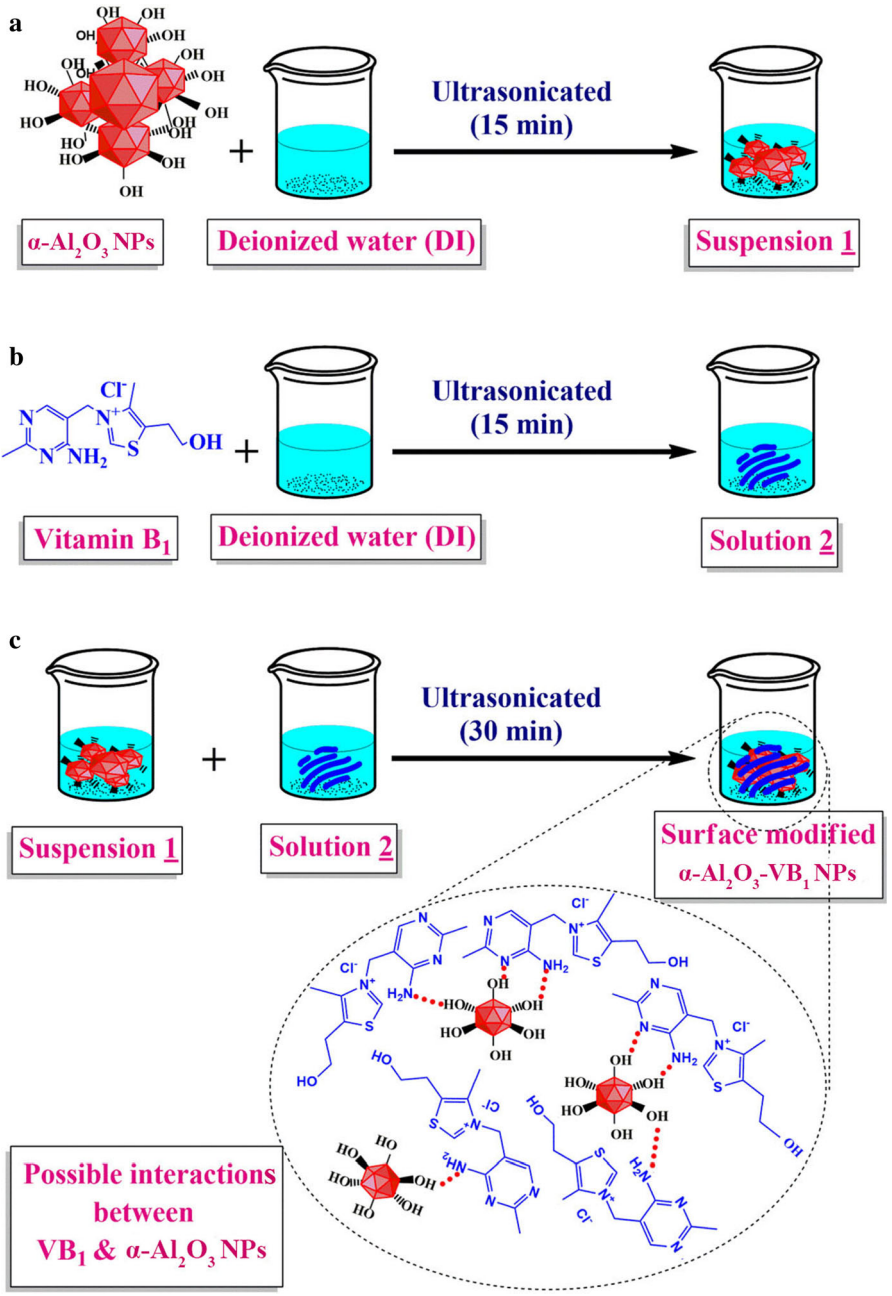

Scheme 1 Surface modification of α-Al_2O_3 with VB_1

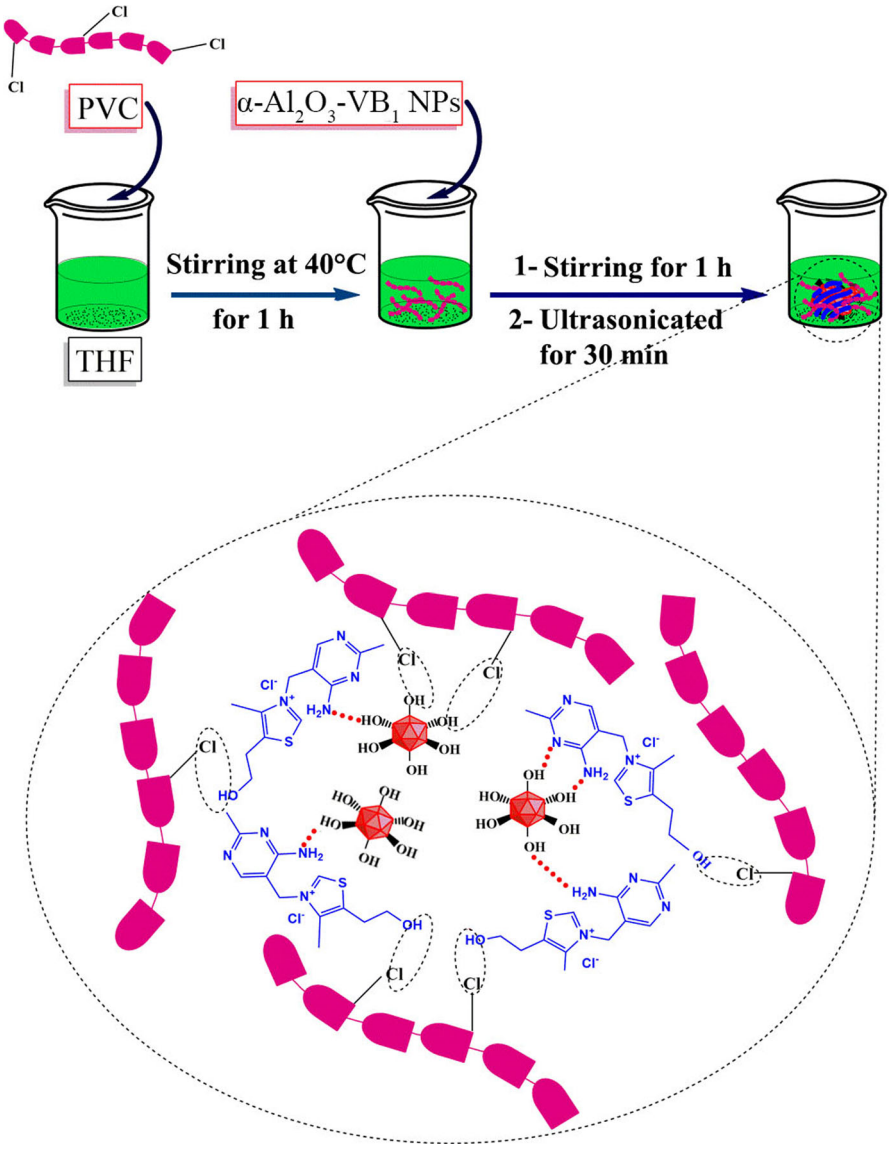

Scheme 2 Preparation of PVC/α-Al_2O_3–VB_1 NC films

FT-IR analysis

Figure 2a presents the FT-IR spectrum of α-Al_2O_3 NPs. The Al–O band is shown at around 400–900 cm^{-1}. The broad peaks at around 3100–3300 and 1600–1700 cm^{-1} correspond to the stretching and bending bonds of hydroxyl groups of adsorbed water molecules on the α-Al_2O_3 surface [34]. Figure 1c exhibits the absorption bands for VB_1. Two peaks around 1615 and 1592 cm^{-1} are assigned to the C=C and

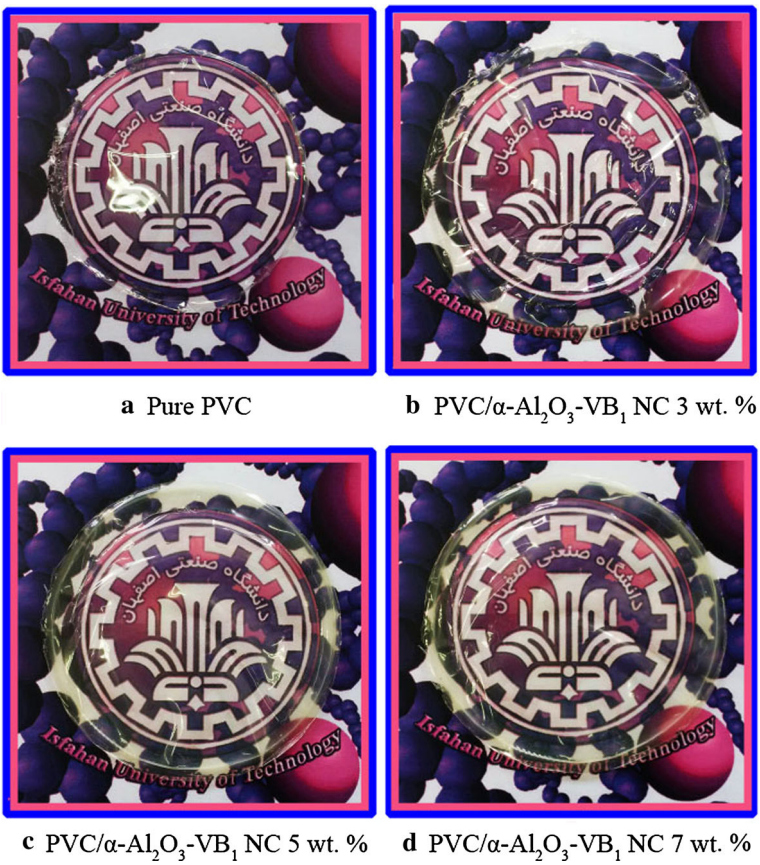

Fig. 1 Photographs of **a** pure PVC, **b** 3 wt.% PVC/α-Al_2O_3–VB_1 NC film, **c** 5 wt.% PVC/α-Al_2O_3–VB_1 NC film, and **d** 7 wt.% PVC/α-Al_2O_3–VB_1 NC film

C=N stretching modes in the pyrimidine structure for VB_1. The peaks at 3424 and 1666 cm^{-1} represent the stretching and bending vibrations of –NH (–NH_2), respectively. An absorbance band at 3492 cm^{-1} corresponded to the O–H stretching. The peak at 3050 cm^{-1} is assigned to the C–H stretching vibrations of the aromatic rings and at 2910 cm^{-1} associated with the aliphatic C–H stretching in VB_1 [35].

The FT-IR spectrum of modified α-Al_2O_3 NPs displays new characteristic peaks (Fig. 2b). The absorption band at 1662 cm^{-1} confirms the existence of VB_1 on the surface of the α-Al_2O_3 NPs; this peak shows that the NH groups of VB_1 appear in α-Al_2O_3–VB_1. The mild shift of absorbance bands toward lower wavenumbers may be ascribed to the interactions between α-Al_2O_3 NPs and VB_1. For instance, the hydrogen bonding between α-Al_2O_3 NPs and VB_1 decreases the frequency of O–H bond from 1637 to 1607 cm^{-1}. The peak at 3431 cm^{-1} can be ascribed to the N–H stretching vibration and confirmed that VB_1 was tied on the α-Al_2O_3 surface [36].

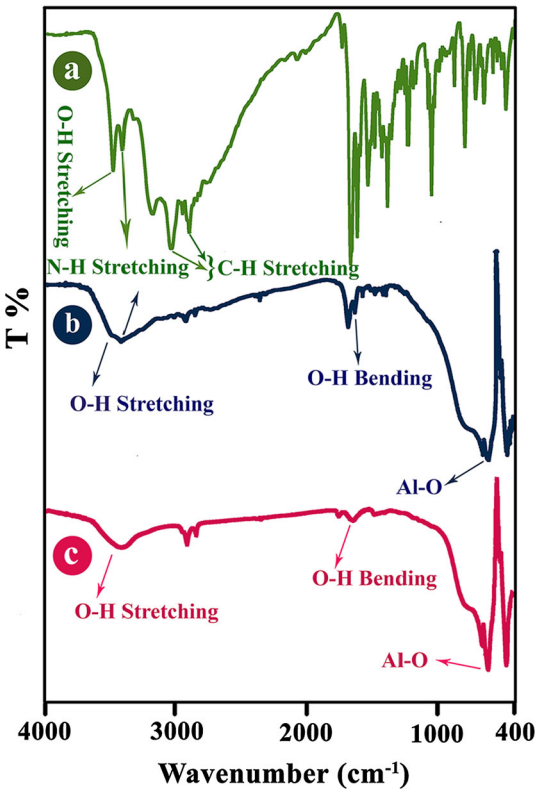

Fig. 2 FT-IR spectra of *a* VB_1, *b* α-Al_2O_3–VB_1 NPs, and *c* α-Al_2O_3 NPs

The spectra of the pure PVC and PVC/α-Al_2O_3–VB_1 NCs are shown in Fig. 3 in absorbance mode. Figure 3a shows the spectrum of pure PVC. The band at 2800–3000 cm^{-1} is attributed to the C–H stretching bond. The peak at 1250 cm^{-1} is assigned to the bending bond of C–H near Cl. The absorbance band in a range of 600–650 cm^{-1} is related to C–Cl gauche bond [37, 38]. In comparison with the pure PVC, new peaks appeared in the spectra of the PVC/α-Al_2O_3–VB_1 NC films (Fig. 3b–d). In addition, the absorption peak of the O–H group at 1607 cm^{-1} shifted to a higher frequency which could be attributed to the formation of effective hydrogen bonds between the α-Al_2O_3–VB_1 NPs and the PVC matrix. The presence of α-Al_2O_3–VB_1 makes changes in the infrared spectrum of pure PVC which attributed to NH group of VB_1 at 1772 cm^{-1}. The band at 425–450 cm^{-1} is in agreement with the Al–O bond. The peak intensity of the α-Al_2O_3 NPs in the PVC/α-Al_2O_3–VB_1 NCs increased with enhancement of the content of modified NPs.

Crystalline structure

XRD was used for the recognition of the crystalline phases. Figure 4 presents the XRD patterns of α-Al_2O_3 NPs and α-Al_2O_3–VB_1 in the 2θ range. The diffraction peaks of α-Al_2O_3 NPs, namely 021, 104, 110, 024, 116, 211, 122, 124, 030, 208, and

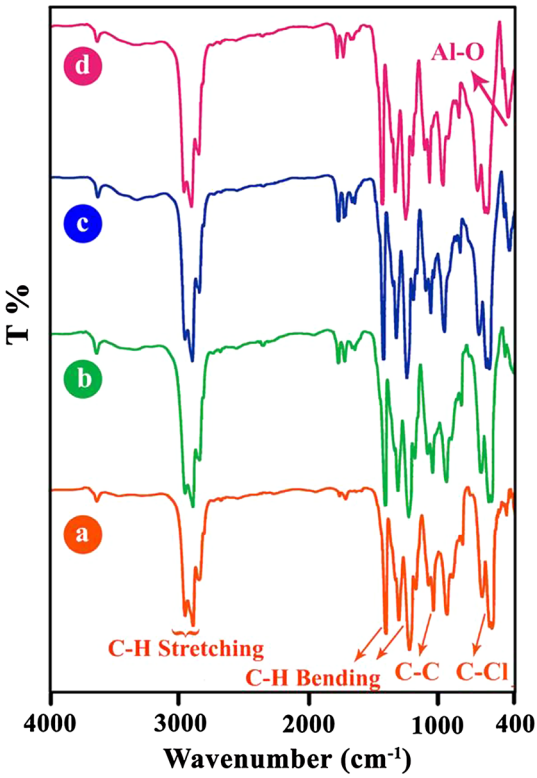

Fig. 3 FT-IR spectra of *a* pure PVC, *b* 3 wt.% PVC/α-Al_2O_3–VB_1 NC film, *c* 5 wt.% PVC/α-Al_2O_3–VB_1 NC film, and *d* 7 wt.% PVC/α-Al_2O_3–VB_1 NC film

119, related to the hexagonal nature of α-Al_2O_3 NPs [39]. These data have good agreement with reported data in the literature. It is seen from the XRD pattern that pure PVC is an amorphous polymer (Fig. 4c) [40]. The XRD curves of PVC/α-Al_2O_3–VB_1 NCs (Fig. 4d–f) indicated a broad peak plus certain peaks that are relevant to NPs' crystalline structure. The XRD patterns of the PVC/α-Al_2O_3–VB_1 NCs demonstrated weak peaks at 2θ, namely 012, 110, 113, 116, and 119 which were slightly raised with increasing the content of the α-Al_2O_3–VB_1 NPs in the PVC matrix. The low intensity of peaks can be attributed to fine dispersion and low percentages of α-Al_2O_3–VB_1 NPs (3, 5, and 7 wt.%) in the polymer matrix [38].

Morphology studies (FE-SEM and TEM)

The morphology of the α-Al_2O_3–VB_1 NPs, pure PVC, and PVC/α-Al_2O_3–VB_1 NC films was observed by FE-SEM micrographs. The FE-SEM images (Fig. 5a) confirmed that the α-Al_2O_3 NPs after modification were nearly spherical in shape, similar to α-Al_2O_3 NPs [41]. The homogenous surface can be observed from FE-SEM micrograph of NC films (Fig. 5c–e). Actually, the ultrasonication caused a uniform surface morphology which ensures a potent interaction between nano-fillers and the matrix [42]. There was no significant change in FE-SEM images of the

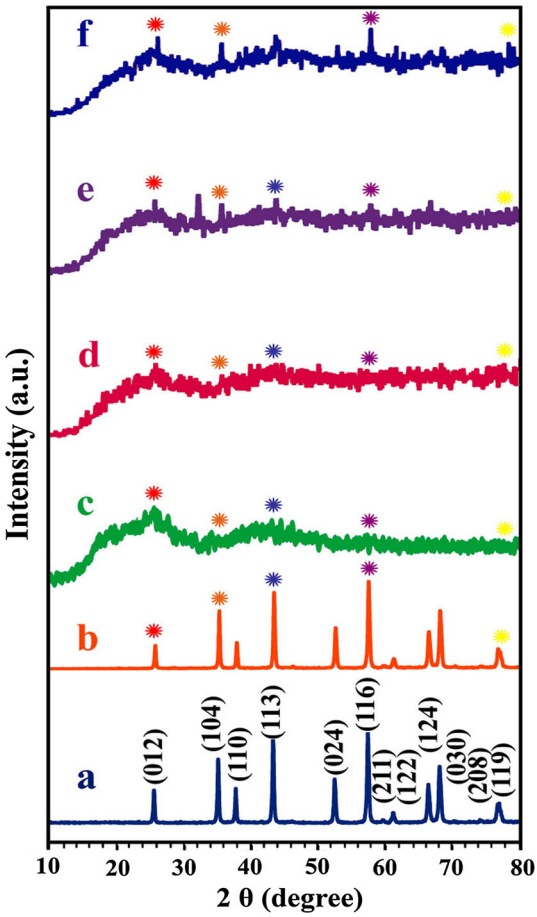

Fig. 4 XRD patterns of *a* α-Al_2O_3 NPs, *b* α-Al_2O_3–VB_1 NPs, *c* pure PVC, *d* 3 wt.% PVC/α-Al_2O_3–VB_1 NC film, *e* 5 wt.% PVC/α-Al_2O_3–VB_1 NC film, and *f* 7 wt.% PVC/α-Al_2O_3–VB_1 NC film

obtained PVC/α-Al_2O_3–VB_1 NCs compared to the pure polymer. For a more detailed observation, TEM analysis was employed.

Clearer morphology and dispersion of NPs into the PVC/α-Al_2O_3–VB_1 NCs were scrutinized by TEM micrographs. As shown in Fig. 6a, modified α-Al_2O_3 NPs display individual spherical-like and single crystalline α-Al_2O_3 NPs with a clean surface [43].

TEM images of the 5 wt.% PVC/α-Al_2O_3–VB_1 NC film at various magnifications are shown in Fig. 6b. These images confirmed the presence of α-Al_2O_3–VB_1 NP in the PVC/α-Al_2O_3–VB_1 NC films. It can be seen that α-Al_2O_3–VB_1 NPs distributed uniformly in the polymer matrix and their sizes decreased. On the one hand, successful modification causes steric effect and separates NPs from each other. On the other hand, ultrasonic irradiations during the formation of NC can break the aggregation of α-Al_2O_3 NPs and cause good dispersion of them in the PVC matrix. It is clear that the size of NPs depends on the ultrasonication time [44]. It is possible that sonication for a long time enhances the chance of the lone particle

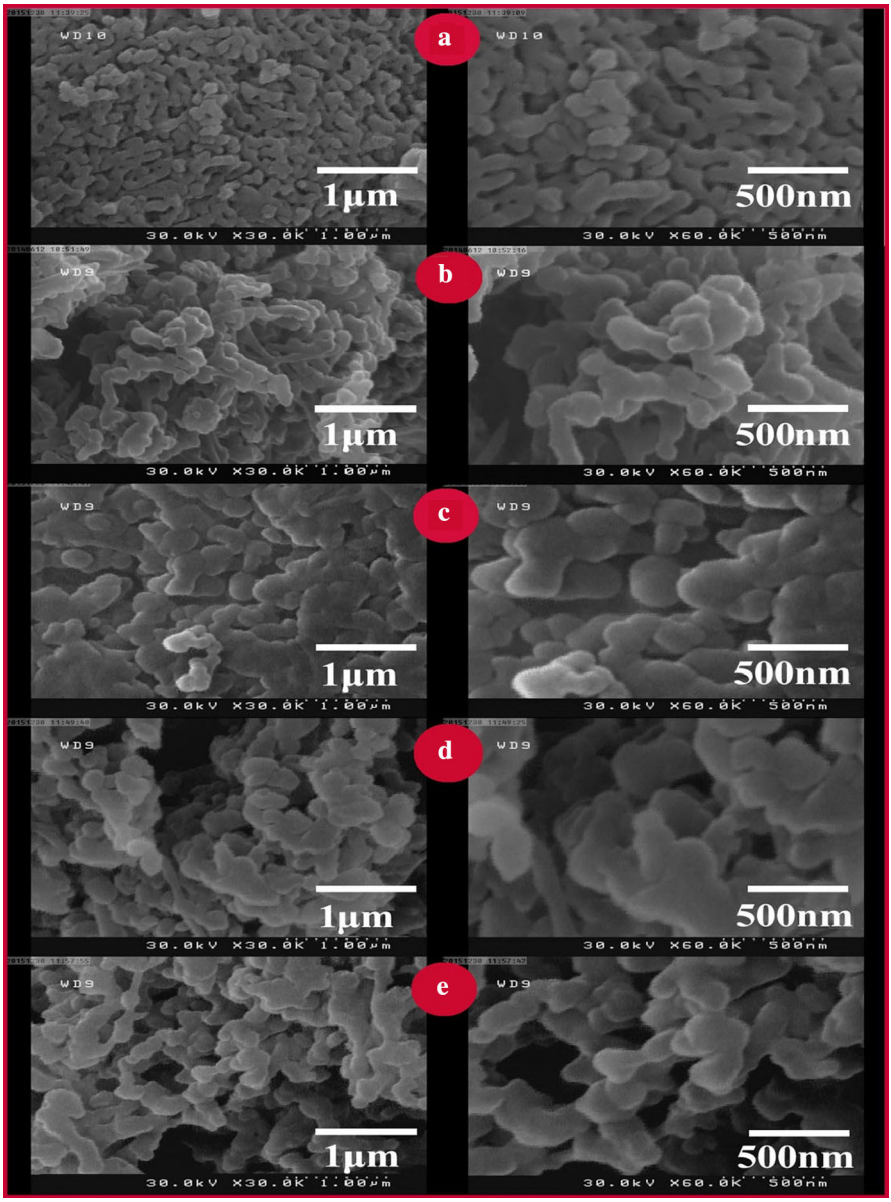

Fig. 5 FE-SEM micrographs of **a** α-Al_2O_3–VB_1 NPs, **b** pure PVC, **c** 3 wt.% PVC/α-Al_2O_3–VB_1 NC film, **d** 5 wt.% PVC/α-Al_2O_3–VB_1 NC film, and **e** 7 wt.% PVC/α-Al_2O_3–VB_1 NC film

reaction with the micro-bubbles produced by the acoustic cavitation. Consequently, due to successful modification as well as ultrasonic irradiations the size of some α-Al_2O_3–VB_1 NPs embedded in the PVC matrix decreased and was found to be 18–30 nm.

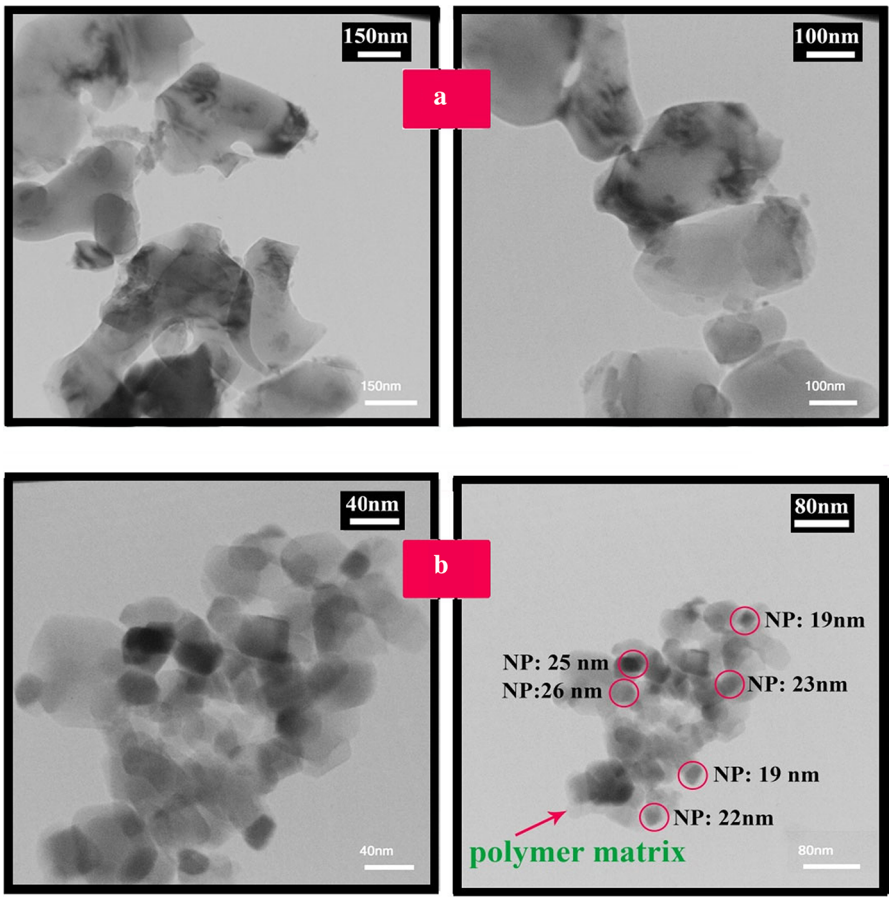

Fig. 6 TEM micrographs of **a** α-Al_2O_3–VB_1 NPs and **b** 5 wt.% PVC/α-Al_2O_3–VB_1 NC film

Combustion test

To estimate the amount of the α-Al_2O_3–VB_1 NPs in the 5 wt.% PVC/α-Al_2O_3–VB_1 NC, it was combusted in air. The images of the 5 wt.% PVC/α-Al_2O_3–VB_1 film before and after combustion from room temperature to 1000 °C and then holding temperature for 4 h at 1000 °C are shown in Fig. 7. It is clear that after combustion, 5 wt.% PVC/α-Al_2O_3–VB_1 film changed to white powder and shows that the remaining materials are metals, which are approximately 5% of the whole weight. It is well known that PVC is a char-forming polymer during combustion. Under strong heat flux, the PVC macromolecules pyrolyze into various smaller molecules and some of these will combust when their concentration reaches some critical value in air [45]. FT-IR analysis was done on residual white powder and it showed characteristic peaks related to α-Al_2O_3 NPs.

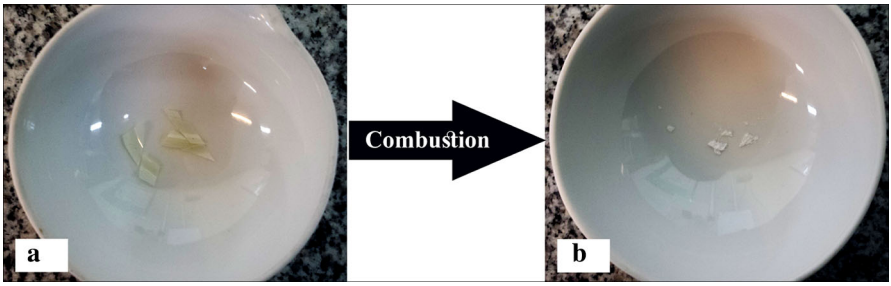

Fig. 7 The digital photographs of 5 wt.% PVC/α-Al_2O_3–VB_1 NC film before and after combustion in air

Thermal stability

The amount of coupling agent is analyzed by TGA thermograms. From Fig. 8b, it can be estimated that the weight ratio of the VB_1 modifier on the α-Al_2O_3 surface is almost 6 wt.%.

TGA curves of the PVC and PVC/α-Al_2O_3–VB_1 NC films are recorded in Fig. 9. For the pure PVC and the NCs, two stages of weight loss were detected. The first transition weight loss of pure PVC from 276 to 298 °C corresponded to the dehydrochlorination. During this first decomposition stage, the sample weight loss is about 55%. Under the effect of temperature, chlorine radicals resulting from scission of –C–Cl labile bonds take off a hydrogen radical from adjacent –C–H groups to form a covalent H–Cl bond. This chemical mechanism induces double bonds along the polymer chain and may lead to conjugated polymeric chains [46]. The sample in the region 298–445 °C becomes thermally stable because of the formation of polyacetylene. The second step of weight loss

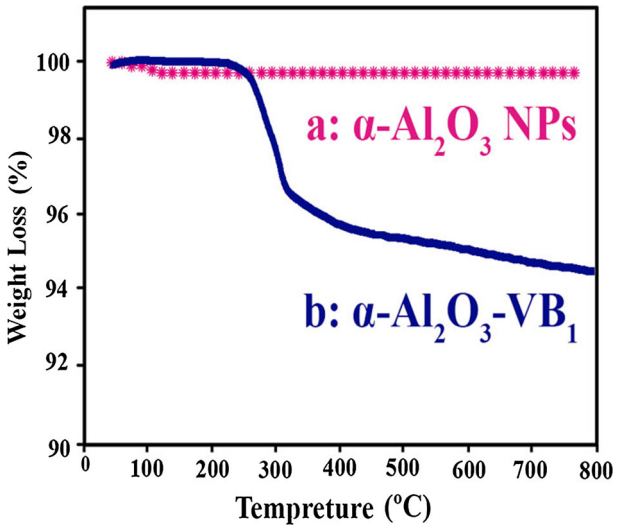

Fig. 8 TGA thermograms of *a* α-Al_2O_3 NPs, *b* α-Al_2O_3–VB_1

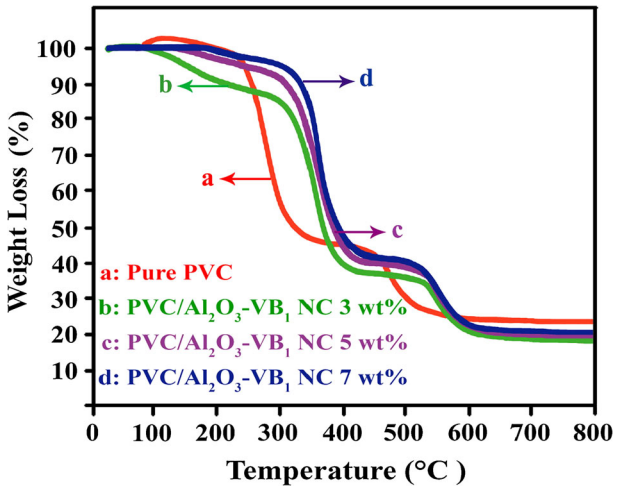

Fig. 9 TGA thermograms of *a* pure PVC, *b* 3 wt.% PVC/α-Al_2O_3–VB_1 NC film, *c* 5 wt.% PVC/α-Al_2O_3–VB_1 NC film, and *d* 7 wt.% PVC/α-Al_2O_3–VB_1 NC film

Table 1 Thermal properties of the pure PVC, 3 wt.% PVC/α-Al_2O_3–VB_1 NC film, 5 wt.% PVC/α-Al_2O_3–VB_1 NC film and 7 wt.% PVC/α-Al_2O_3–VB_1 NC film

Samples	T_5 (°C)[a]	T_{10} (°C)[b]	Char yield (%)[c]
Pure PVC	240.3	254.8	23.3
PVC/α-Al_2O_3–VB_1 NC film, 3 wt.%	154.5	217.9	18.2
PVC/α-Al_2O_3–VB_1 NC film, 5 wt.%	244.4	308.8	20.0
PVC/α-Al_2O_3–VB_1 NC film, 7 wt.%	304.3	332.9	20.7

[a] Temperature at which 5 wt.% weight loss was recognized by TGA at a heating rate of 20 °C min^{-1} in an argon atmosphere

[b] Temperature at which 10 wt.% weight loss was verified by TGA at a heating rate of 20 °C min^{-1} in an argon atmosphere

[c] Percentage weight of the material left undecomposed after TGA analysis at 800 °C in an argon atmosphere

in the range of 445–530 °C is probably a consequence of the polyacetylene cracking [47].

The resulting TGA data including temperatures at 5% (T_5) and 10% (T_{10}) weight loss, and char yield (CY) at 800 °C are summarized in Table 1.

As it can be seen, the TGA curves of the PVC/α-Al_2O_3–VB_1 NCs shifted to higher temperatures than the pure PVC. After addition of α-Al_2O_3–VB_1, the T_5 and T_{10} values of 5 and 7 wt.% NCs were improved.

UV–Vis absorption

As shown in Fig. 10, pure PVC and PVC NCs display strong absorption in UV region. The spectrum of pure PVC showed absorbance peaks at $\lambda = 210$ and

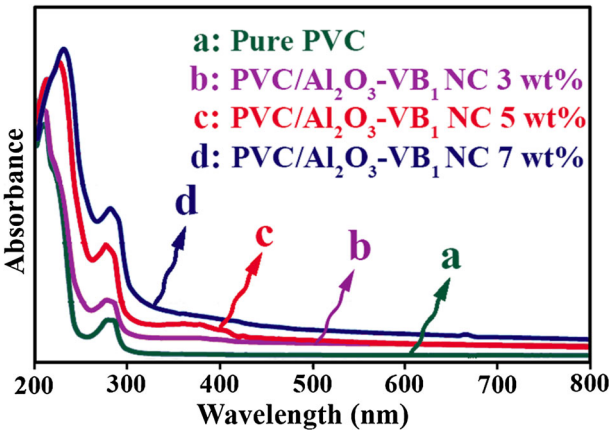

Fig. 10 UV–Vis absorption spectra of *a* pure PVC, *b* 3 wt.% PVC/α-Al_2O_3–VB_1 NC film, *c* 5 wt.% PVC/α-Al_2O_3–VB_1 NC film, and *d* 7 wt.% PVC/α-Al_2O_3–VB_1 NC film

280 nm, which can be assigned to the $n \rightarrow \pi^*$ and $\pi \rightarrow \pi^*$ transitions, respectively [48]. The α-Al_2O_3 NPs have UV–Vis absorption at $\lambda = 205$ nm [49] which has been covered by adsorption peak related to PVC. Therefore, the absorption intensity of PVC/α-Al_2O_3–VB_1 NCs increased with increasing the content of the α-Al_2O_3–VB_1 NPs in the PVC matrix.

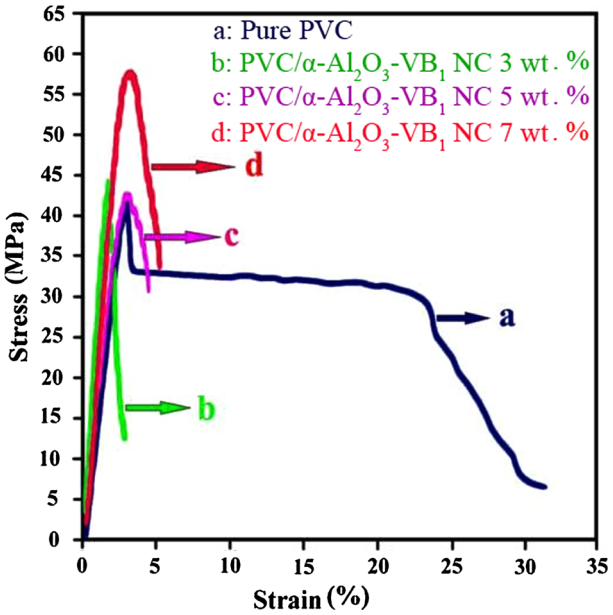

Fig. 11 Mechanical properties of *a* pure PVC, *b* 3 wt.% PVC/α-Al_2O_3–VB_1 NC film, *c* 5 wt.% PVC/α-Al_2O_3–VB_1 NC film, and *d* 7 wt.% PVC/α-Al_2O_3–VB_1 NC film

Mechanical properties

The stress–strain curves of pure PVC film and PVC/α-Al_2O_3–VB_1 NCs are depicted in Fig. 11 and the corresponding tensile strength, Young's modulus, elongation, and strain are summarized in Table 2. The mechanical properties of PVC/α-Al_2O_3–VB_1 NCs can be affected by many factors, such as the morphology, size, loading, distribution, and interfacial adhesion of NPs [30, 47].

Table 2 shows that stress, strain, and elongation increased for NCs of 5 and 7 wt.%. This can be explained by the reason that the incorporation of α-Al_2O_3–VB_1 NPs into the PVC matrix effectively enhanced the interfacial interactions between NPs and matrix via the establishment of hydrogen and covalent bonds between them. The interfacial bonding between NPs and matrix can effectively transfer the applied stress to the α-Al_2O_3 NPs and improve the mechanical properties [38].

Water contact angle analysis

Hydrophilicity of a polymer surface is an important property for biomedical application [50]. It is well known that alumina has a hydrophilic surface [51]; therefore, the effect of the presence of α-Al_2O_3–VB_1 NPs on the hydrophilicity of

Table 2 Mechanical properties from tensile testing for pure PVC and PVC/α-Al_2O_3–VB_1 NC film

Samples	Stress (MPa)	Strain (%)	Young's modulus (GPa)	Elongation at max (mm)
Pure PVC	42.14	2.68	1.87	0.94
PVC/α-Al_2O_3–VB_1 NC film, 3 wt.%	43.82	1.62	2.64	0.57
PVC/α-Al_2O_3–VB_1 NC film, 5 wt.%	42.16	2.71	1.43	0.95
PVC/α-Al_2O_3–VB_1 NC film, 7 wt.%	57.3	2.74	1.98	0.96

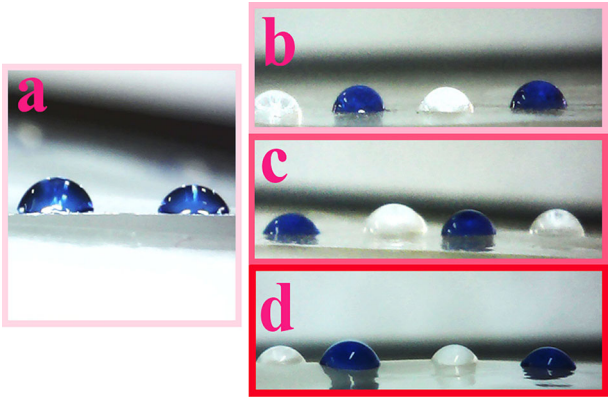

Fig. 12 Images of water droplets on *a* pure PVC, *b* 3 wt.% PVC/α-Al_2O_3–VB_1 NC film, *c* 5 wt.% PVC/α-Al_2O_3–VB_1 NC film, and *d* 7 wt.% PVC/α-Al_2O_3–VB_1 NC film

Table 3 Water static contact angles for pure PVC and PVC/α-Al_2O_3–VB_1 NC films

Samples	Contact angles
Pure PVC	80.02 ± 1.76
PVC/α-Al_2O_3–VB_1 NC film, 3 wt.%	75.05 ± 1.06
PVC/α-Al_2O_3–VB_1 NC film, 5 wt.%	73.15 ± 1.21
PVC/α-Al_2O_3–VB_1 NC film, 7 wt.%	65.42 ± 1.75

NCs was analyzed in this study. Water droplets on the pure PVC and PVC/α-Al_2O_3–VB_1 NC films are shown in Fig. 12. In addition, water static contact angles were measured and are summarized in Table 3. The decrease in contact angles of NCs compared to the pure PVC can be ascribed to the presence of abundant hydroxyl groups on the surface of α-Al_2O_3–VB_1 NPs which increases ability of PVC surface to form hydrogen bonds with water molecules (Fig. 12).

Conclusions

In this study we considered a simple and efficient method to obtain the PVC/α-Al_2O_3–VB_1 NC films with improved thermal and mechanical properties. The ultrasonic technique was used for the synthesis of the NCs in a green and simple way. The α-Al_2O_3 NPs were treated by VB_1 as a biocompatible modifier to enhance homogeneous dispersion and reduce the aggregation in the matrix. Then, the PVC NCs were prepared with different percentages of α-Al_2O_3–VB_1 NPs (3, 5, and 7 wt.%). FE-SEM and TEM images were used to study the distribution of NPs and uniform morphology of the PVC/α-Al_2O_3–VB_1 NCs. The XRD patterns of PVC/α-Al_2O_3–VB_1 NCs indicated that the crystalline phase of α-Al_2O_3 NP was not changed. A comparison of T_5 and T_{10} of the PVC/α-Al_2O_3–VB_1 NCs with pure PVC showed an increase in thermal stability of 5 and 7 wt.% PVC/α-Al_2O_3–VB_1 NCs. The UV absorbance of PVC/α-Al_2O_3–VB_1 NCs is raised with increasing the content of the α-Al_2O_3–VB_1 NPs in the PVC matrix. The prepared PVC/α-Al_2O_3–VB_1 NC films can be used to block the UV radiation (at about 280 nm). Water static contact angles were investigated and showed hydrophilicity enhancement of PVC/α-Al_2O_3–VB_1 NCs. As a result, it can be mentioned that the presence of VB_1 as modifier agent can prevent the agglomeration of α-Al_2O_3 NPs and cause a positive impact on thermal, mechanical, and optical properties of PVC/α-Al_2O_3–VB_1 NCs. Due to high mechanical properties and UV absorption ability of the obtained composite films, they may be employed in packaging applications.

Acknowledgements The authors would like to express their acknowledgment to the Research Affairs Division Isfahan University of Technology (IUT), Isfahan, Iran, for partial financial support. In addition, the authors are thankful to Iran Nanotechnology Initiative Council (INIC), Tehran, Iran, National Elite Foundation (NEF), Tehran, Iran and Center of Excellence in Sensors and Green Chemistry (IUT).

References

1. Mallakpour S, Khadem E (2016). Chapter 16 recent achievements in the synthesis of biosafe poly(vinyl alcohol) nanocomposite. In: Inamuddin (ed) Green polymer composites technology; properties and applications. Taylor & Francis Group, 6000 Broken Sound Parkway NW, Suite 300, Boca Raton, FL 33487-2742 CRC Press, pp 261–278. doi:10.1201/9781315371184-17
2. Stanković A, Dimitrijević S, Uskoković D (2013) Influence of size scale and morphology on antibacterial properties of ZnO powders hydrothermally synthesized using different surface stabilizing agents. Colloids Surf B 102:21–28
3. Cava S, Tebcherani S, Souza I, Pianaro S, Paskocimas C, Longo E, Varela JA (2007) Structural characterization of phase transition of Al_2O_3 nanopowders obtained by polymeric precursor method. Mater Chem Phys 103(2):394–399
4. Kar KK, Srivastava S, Rahaman A, Nayak S (2008) Acrylonitrile-butadiene-styrene nanocomposites filled with nanosized alumina. Polym Compos 29(5):489–499
5. Mallakpour S, Dinari M (2013) Enhancement in thermal properties of poly(vinyl alcohol) nanocomposites reinforced with Al_2O_3 nanoparticles. J Reinf Plast Compos 32(4):217–224
6. Mahdavian AR, Sarrafi Y, Shabankareh M (2009) Nanocomposite particles with core–shell morphology III: preparation and characterization of nano Al_2O_3–poly(styrene–methyl methacrylate) particles via miniemulsion polymerization. Polym Bull 63(3):329–340
7. Mallakpour S, Javadpour M (2016) Chapter 35 design strategies of green polymer nanocomposites containing amino acid linkages. In: Inamuddin (ed) Green polymer composites technology. Taylor & Francis Group, 6000 Broken Sound Parkway NW, Suite 300, Boca Raton, FL 33487-2742 CRC Press, pp 491–512. doi:10.1201/9781315371184-36
8. Sperling RA, Parak W (2010) Surface modification, functionalization and bioconjugation of colloidal inorganic nanoparticles. Philos Trans R Soc Lond A Math Phys Eng Sci 368(1915):1333–1383
9. Smuleac V, Butterfield D, Sikdar S, Varma R, Bhattacharyya D (2005) Polythiol-functionalized alumina membranes for mercury capture. J Membr Sci 251(1):169–178
10. Branch M (2011) Preparation of nano-scale α-Al_2O_3 powder by the sol-gel method. Ceram Silikáty 55(4):378–383
11. Iijima M, Kamiya H (2009) Surface modification for improving the stability of nanoparticles in liquid media. KONA Powder Part J 27:119–129
12. Mallakpour S, Madani M (2015) A review of current coupling agents for modification of metal oxide nanoparticles. Prog Org Coat 86:194–207
13. Gaume J, Taviot-Gueho C, Cros S, Rivaton A, Therias S, Gardette J-L (2012) Optimization of PVA clay nanocomposite for ultra-barrier multilayer encapsulation of organic solar cells. Sol Energy Mater Sol Cells 99:240–249
14. Mallakpour S, Nezamzadeh Ezhieh A (2015) A simple and environmentally friendly method for surface modification of ZrO_2 nanoparticles by biosafe citric acid as well as ascorbic acid (vitamin C) and its application for the preparation of poly(vinyl chloride) nanocomposite films. Polym Compos. doi:10.1002/pc.23746
15. Beitollahi A, Hosseini-Bay H, Sarpoolaki H (2010) Synthesis and characterization of Al_2O_3–ZrO_2 nanocomposite powder by sucrose process. J Mater Sci Mater Electron 21(2):130–136
16. Zhou Y, Fu S, Zheng L, Zhan H (2012) Effect of nanocellulose isolation techniques on the formation of reinforced poly(vinyl alcohol) nanocomposite films. Express Polym Lett 6(10):794–804
17. Khanna P, Singh N, Charan S, Subbarao V, Gokhale R, Mulik U (2005) Synthesis and characterization of Ag/PVA nanocomposite by chemical reduction method. Mater Chem Phys 93(1):117–121
18. Sairam M, Patil MB, Veerapur RS, Patil SA, Aminabhavi TM (2006) Novel dense poly(vinyl alcohol)–TiO_2 mixed matrix membranes for pervaporation separation of water–isopropanol mixtures at 30 C. J Membr Sci 281(1):95–102
19. Paranhos CM, Soares BG, Oliveira RN, Pessan LA (2007) Poly(vinyl alcohol)/clay-based nanocomposite hydrogels: swelling behavior and characterization. Macromol Mater Eng 292(5):620–626
20. Mallakpour S, Hatami M (2016) Condensation polymer/layered double hydroxide NCs: preparation, characterization, and utilizations. Eur Polym J 90:273–300. doi:10.1016/j.eurpolymj.2017.03.015
21. Mallakpour S, Soltanian S (2010) Studies on syntheses and morphology characteristic of chiral novel poly(ester-imide)/TiO_2 bionanocomposites derived from L-phenylalanine based diacid. Polymer 51(23):5369–5376

22. Jokar A, Azizi MH, Hamidi Esfehani Z (2015) Effects of ultrasound time on the properties of poly(vinyl alcohol-based) nanocomposite films. Nutr Food Sci Res 2(4):29–38
23. Singh NG, Lily M, Devi SP, Rahman N, Ahmed A, Chandra AK, Nongkhlaw R (2016) Synthetic, mechanistic and kinetic studies on the organo-nanocatalyzed synthesis of oxygen and nitrogen containing spiro compounds under ultrasonic conditions. Green Chem 18(15):4216–4227
24. Leopold N, Cîntă-Pînzaru S, Baia M, Antonescu E, Cozar O, Kiefer W, Popp J (2005) Raman and surface-enhanced Raman study of thiamine at different pH values. Vib Spectrosc 39(2):169–176
25. Lei M, Ma L, Hu L (2009) Thiamine hydrochloride as a efficient catalyst for the synthesis of amidoalkyl naphthols. Tetrahedron Lett 50(46):6393–6397
26. Albeniz S, Vicente M, Trujillano R, Korili S, Gil A (2014) Synthesis and characterization of organosaponites. Thermal behavior of their poly(vinyl chloride) nanocomposites. Appl Clay Sci 99:72–82
27. Yang C, Tian L, Ye L, Peng T, Deng K, Zan L (2011) Enhancement of photocatalytic degradation activity of poly(vinyl chloride)-TiO2 nanocomposite film with polyoxometalate. J Appl Polym Sci 120(4):2048–2053
28. Elashmawi I, Hakeem N, Marei L, Hanna F (2010) Structure and performance of ZnO/PVC nanocomposites. Phys B 405(19):4163–4169
29. Wang Q, Jang M, Chen YF (2007) Effects of nanosized iron oxide with different morphology on nanomechanical properties of nanocomposite coating. Key Eng Mater 336–338:2218–2220
30. Saadatabadi NM, Nateghi MR, Borhanizarandi M (2014) Fabrication and characterization of nanosilver intercalated graphene embedded poly(vinyl chloride) composite thin films. J Polym Res 21(8):1–9
31. Mallakpour S, Behranvand V (2016) Grafted nano-ZnO, TiO_2 and CuO by biosafe coupling agents and their applications for the green polymer nanocomposites fabrication. In: Inamuddin (ed) Green polymer composites technology: properties and applications, chap 24. CRC Press, Taylor & Francis Group, Boca Raton, pp 381–396
32. Chen J, Zhou Y, Nan Q, Sun Y, Ye X, Wang Z (2007) Synthesis, characterization and infrared emissivity study of polyurethane/TiO_2 nanocomposites. Appl Surf Sci 253:9154–9158
33. Abdul Nabi M, Yusop RM, Yousif E, Abdullah BM, Salimon J, Salih N, Zubairi SI (2014) Effect of nano ZnO on the optical properties of poly(vinyl chloride) films. Int J Polym Sci. doi:10.1155/2014/697809
34. Ghezelbash Z, Ashouri D, Mousavian S, Ghandi AH, Rahnama Y (2012) Surface modified Al_2O_3 in fluorinated polyimide/Al_2O_3 nanocomposites: synthesis and characterization. Bull Mater Sci 35(6):925–931
35. Carraher CE Jr, Roner MR, Lambert RE, Arroyo L, Miller LC (2015) Synthesis of organotin polyamine ethers containing thiamine (vitamin B_1) and preliminary ability to inhibit select cancer cell lines. J Inorg Organomet Polym Mater 25(6):1414–1424
36. Azizi K, Heydari A (2014) Vitamin B_1 supported on silica-encapsulated γ-Fe_2O_3 nanoparticles: design, characterization and application as a greener biocatalyst for highly efficient acylation. RSC Adv 4(17):8812–8816
37. Dunbai Z, Changgen C, Demin J (2006) Preparation and mechanical properties of solid-phase grafting nanocomposites of PVC/graft copolymers/MMT. J Wuhan Univ Technol Mater Sci Ed 21(4):5–8
38. Mallakpour S, Abdolmaleki A, Tabebordbar H (2016) Production of PVC/α-MnO_2-KH550 nanocomposite films: morphology, thermal, mechanical and Pb(II) adsorption properties. Eur Polymer J 78:141–152
39. Mallakpour S, Dinari M (2013) The synergetic effect of chiral organoclay and surface modified-Al_2O_3 nanoparticles on thermal and physical properties of poly(vinyl alcohol) based nanocomposite films. Prog Org Coat 76(1):263–268
40. Vasanthkumar M, Bhatia R, Arya VP, Sameera I, Prasad V, Jayanna H (2014) Characterization, charge transport and magnetic properties of multi-walled carbon nanotube–polyvinyl chloride nanocomposites. Phys E 56:10–16
41. Kamil F, Hubiter K, Abed T, Al-Amiery A (2015) Synthesis of aluminum and titanium oxides nanoparticles via sol-Gel method: optimization for the minimum size. J Nanosci Technol 37–39
42. Mallakpour S, Behranvand V (2016) Manufacture and characterization of nanocomposite materials obtained from incorporation of D-glucose functionalized MWCNTs into the recycled poly(ethylene terephthalate). Des Monomers Polym 19(4):283–289

43. Li H, Li Y, Jiao J, Hu H-M (2011) Alpha-alumina nanoparticles induce efficient autophagy-dependent cross-presentation and potent antitumour response. Nat Nanotechnol 6(10):645–650
44. Li W, Yue J, Liu S (2012) Preparation of nanocrystalline cellulose via ultrasound and its reinforcement capability for poly (vinyl alcohol) composites. Ultrason Sonochem 19(3):479–485
45. Wang Q, Zhang X, Jin Y, Gui H, Dong W, Lai J, Liu Y, Gao J, Huang F, Song Z (2006) Preparation and properties of PVC ternary nanocomposites containing elastomeric nanoscale particles and exfoliated sodium-montmorillonite. Macromol Mater Eng 291(6):655–660
46. Bishay I, Abd-El-Messieh S, Mansour S (2011) Electrical, mechanical and thermal properties of poly(vinyl chloride) composites filled with aluminum powder. Mater Des 32(1):62–68
47. Yuan W, Cui J, Cai Y, Xu S (2015) A novel surface modification for calcium sulfate whisker used for reinforcement of poly(vinyl chloride). J Polym Res 22(9):1–9
48. Hasan M, Kumar R, Barakat M, Lee M (2015) Synthesis of PVC/CNT nanocomposite fibers using a simple deposition technique for the application of Alizarin Red S (ARS) removal. RSC Advances 5(19):14393–14399
49. Kortov V, Nikiforov S, Milman I, Moiseykin E (2004) Specific features of luminescence of radiation-colored α-Al_2O_3 single crystals. Radiat Meas 38(4):451–454
50. Choinska E, Muroya T, Swieszkowski W, Aoyagi T (2016) Influence of macromolecular structure of novel 2-and 4-armed polylactides on their physicochemical properties and in vitro degradation process. J Polym Res 23(7):1–11
51. Deki S, Kajinami A, Kanaji Y, Mizuhata M, Nagata K (1993) Properties of CaCl2 hydrate with an inorganic powder. Part 2. —Melting behaviour and thermodynamic properties of CaCl2 nH2O (n = 6.00–7.35) with α-Al2O3 or α-SiC powder. J Chem Soc Faraday Trans 89(20):3811–3815